Mechanisms and Modeling of Bake-Hardening Steels: Part I. Uniaxial Tension

V. BALLARIN, M. SOLER, A. PERLADE, X. LEMOINE, and S. FOREST

A physically based model for bake-hardening (BH) steels is developed suitable to predict the BH as well as the macroscopic behavior of strain-aged steels in tensile tests, such as the lower yield stress and the yield point elongation or Lüders strain. A description of the strain aging kinetics is given by considering two aging steps: Cottrell atmospheres formation and precipitation of coherent carbides. The modeling includes the effect of solute carbon content, aging time, temperature, and prestrain. Then, a numerical approach of Lüders phenomenon using finite element (FE) method codes is conducted. The strain aging model is eventually coupled with the previous numerical study thanks to a local mechanical behavior that schematically describes the local dislocation behavior. Simulations of tensile tests are performed and agree well with experiments carried out on aluminum-killed (AlK) and ULC BH steels, in terms of lower yield stress and yield point elongation. Effects of aging treatment, grain size, and strain rate on the macroscopic behavior are particularly enlightened.

DOI: 10.1007/s11661-009-9813-5

I. INTRODUCTION

REQUIREMENTS of increased dent resistance of steels in the automotive industry have largely contributed to the development of new bake-hardening (BH) ultra-low-carbon steels (ULC). These low-strength deep drawing steels initially offer low yield strength before forming, but they exhibit an increased yield strength after forming and paint baking in automotive manufacturing. This strengthening is due to work hardening during sheet forming processes and to BH during paint-baking processes. The latter phenomenon corresponds to strain aging, which is the interaction between solute carbon and dislocations.[1] Recent BH steels initially present a relatively low dislocation density and a controlled level of carbon in solution, so that the strain aging phenomenon only occurs during the paint-baking process. Diffusion of carbon leads to formation of Cottrell atmospheres[1] and pinning of dislocations. If subsequent strain occurs after stamping and baking, the material exhibits higher yield strength but also the return of a sharp yield point during tensile tests. In that case, plastic instabilities called Piobert–Lüders bands propagate along the testpiece. This corresponds to a localization of plastic strain, which leads to a plateau on the macroscopic stress-strain response.

V. BALLARIN, Research Engineer, is with the Automotive Applications Research Center, Arcelor-Mittal Montataire, 60761 Montataire, France. M. SOLER, A. PERLADE, and X. LEMOINE, Research Engineers, are with the Automotive Products Research Center, Arcelor-Mittal Maizières, Voie Romaine, 57283 Maizières-lès-Metz, France. Contact e-mail: xavier.lemoine@arcelormittal.com S. FOREST, CNRS Research Director, is with Mines ParisTech, Centre des Matériaux, UMR CNRS 7633, 91003 Evry Cedex, France.
Manuscript submitted October 16, 2007.
Article published online April 15, 2009

Descriptions of bake hardenability are usually based on uniaxial tensile tests. First, a specimen is loaded to 2 pct strain, which is a typical amount of strain received by outer panels during stamping. Then, the specimen is baked at 170 °C for 20 minutes to simulate the industrial paint-baking process. Finally, the prestrained and baked specimen is uniaxially tested in the same direction as the prestrain. The BH is defined as the difference between the lower yield stress after baking and the final flow stress after prestraining, as displayed in Figure 1.

This phenomenon has been widely studied in the literature. From a metallurgical point of view, strain aging, mainly due to Cottrell atmosphere formation, is influenced by numerous and often coupled parameters,[2,3] mainly the chemical composition and especially the solid solution carbon content, the grain size, and the aging conditions (temperature and time). For instance, grain size plays a particular role on solute carbon content, but the resulting effect on BH is not very well understood.[2]

The Piobert–Lüders phenomenon has also been investigated from a mechanical point of view. Models have been developed to explain the rapid mobile dislocation multiplication occurring after the material yields.[4–7] The effect of strain rate and grain size was often taken into account by examining the Lüders band velocity. Butler[8] particularly focused on grain size and showed its effect on Lüders plateau characteristics and bands velocity. The conclusion was that, for small grain size, band velocity decreases and Lüders stress increases.

Eventually, a detailed understanding of both the kinetics of strain aging and plastic instabilities propagation is then required to model the behavior of such complex steels during tensile tests. Moreover, investigations have to be carried out to study the effect of aging on strain path changes in order to predict the effect of BH on dent resistance.

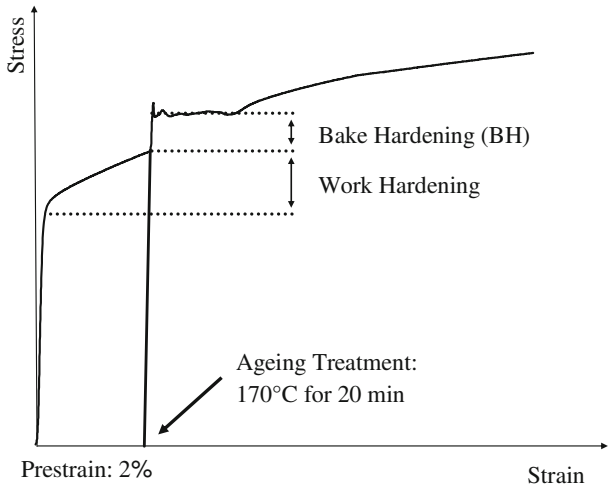

Fig. 1—Schematic diagram of a standard test and definition of the BH.

The aim of the study is twofold: propose a model to predict the static strain aging behavior of BH steel during tensile tests and investigate the strain-path change dependence of BH. Therefore, the present work is divided into two parts. The first part is devoted to a physical-based modeling for BH steels suitable to predict the BH and the macroscopic behavior of strain-aged steels in tensile tests. The companion article[9] deals with BH strain-path dependence and its modeling in order to simulate dent tests.

This work is based on experiments carried out on two BH steels. Effects of solute carbon content, grain size, aging treatment, and prestrain are particularly investigated. Static strain aging is then modeled. First, the physical phenomenon of strain aging based on Cottrell atmospheres formation and precipitation of coherent carbides is studied. A detailed description of the strain aging kinetics is given based on a generalized form of the Harper model[10] taking into account the diffusion of carbon atoms in the stress field of a dislocation, progressive carbon depletion from the matrix, and saturation of the available dislocation sites. Then, a local mechanical model describing schematically the evolution of dislocation density is introduced in a finite element (FE) code. Simulations are eventually performed and compared with experiments.

II. MATERIALS AND EXPERIMENTAL PROCEDURES

Experiments were conducted on two BH steels, an aluminum-killed (AlK) one and a Ti-stabilized ULC one. The chemical compositions of the steels are detailed in Table I. Sheets were received after hot rolling; they were given 80 pct cold reduction and then annealed at 800 °C for 1 minute. The grain sizes obtained were 12 μm for the AlK grade and 13 μm for the ULC one. Additional treatments were carried out in order to control the level of carbon in solution. Three different solute carbon contents (20, 40, and 60 ppm) were obtained for the AlK steel and one (20 ppm) for the ULC one. To investigate the effect of grain size, three different cold rolling rates (20, 75, and 90 pct) were performed on the AlK steel in order to get three different grain sizes (30, 13, and 8 μm) but with the same solute carbon content (20 ppm). Eventually, all AlK modalities were temper rolled 1.5 pct and ULC 2 pct in order to remove any sharp yield point. Typical mechanical behaviors of both steels widely used in this work are given in Table II.

Tensile specimens were prepared from the sheets and prestrained at 2 pct for AlK modalities, 2 and 5 pct for the ULC modality. Aging treatments were carried out at 120 °C and 170 °C for various aging times. Testpieces were then restrained in the same direction as prestrain to failure. Measured BH is defined as the difference between the lower yield stress after aging and the flow stress at the end of the prestraining, as displayed in Figure 1.

Additional tests were performed to measure the carbon content in solution. A thermoelectric power system was used to check the level of solute carbon during modalities elaboration and to analyze solute carbon evolutions after the aging treatments.

III. MODELING

A. *Strain Aging Model*

In order to describe the physical phenomenon of strain aging, the formation of Cottrell atmospheres must be examined. The components of such a model are the following: (1) prediction of solute carbon content, which is necessary for dislocation pinning; (2) prediction of

Table I. Chemical Composition (Weight Percent), Solute Carbon Content (ppm), and Grain Size (μm) of the Steels

Steel	C	Mn	P	Si	S	N	Al	Ti	Css (ppm)	d (μm)
AlK	0.021	0.173	0.005	0.007	0.007	0.005	0.048	0	20	12
ULC	0.002	0.478	0.006	0.006	0.008	0.003	0.034	0.016	22	13

Table II. Mechanical Properties of the Steels*

Steel	YS (MPa)	UTS (MPa)	YPE (Pct)	UE (Pct)	TE (Pct)
AlK	183	320	0	21.8	42
ULC	191	312	0	22.5	40.2

YS is yield strength, UTS is ultimate tensile strength, YPE is yield point elongation, UE is uniform elongation, and TE is total elongation.

dislocation density; and (3) determination of strain aging kinetics.

In the first part, the solute carbon content necessary for dislocation pinning is predicted by considering the supersaturation of solute carbon and intergranular segregation during the annealing following the model proposed by Mac Lean.[11]

The forest dislocation density ρ_f after prestrain is evaluated from the competition between accumulation and annihilation by dynamic recovery, so that

$$\frac{\partial \rho_f}{\partial \varepsilon_p} = \frac{M}{\mathbf{b}d} - Mf \cdot \rho_f \qquad [1]$$

where M is the Taylor factor, d is the ferritic grain size, $\mathbf{b}$ is the Burgers vector, f is a coefficient measuring the intensity of dynamic recovery, and ε_p is the plastic strain.

If ρ_{f_0} represents the initial dislocation density, that is to say the dislocation density after skin pass, the previous equation can be integrated as

$$\rho_f = \rho_{f_0} \cdot \exp(-fM\varepsilon_p) + \frac{1 - \exp(-fM\varepsilon_p)}{\mathbf{b}fd} \qquad [2]$$

According to Bergström[12] and Kocks,[13] one can then relate the flow stress σ to the forest dislocation density and determine the plastic flow behavior of the steel before aging:

$$\sigma = \sigma_0 + \alpha G \mathbf{b} \sqrt{\rho_f} \qquad [3]$$

where σ_0 is the friction stress, α a proportionality factor, and G the shear modulus.

A detailed description of the strain aging kinetics is given based on a generalized form of the Harper model.[10] This description takes into account the diffusion of carbon atoms in the stress field of a dislocation, the progressive carbon depletion in the matrix, and the saturation of the available dislocation sites, as already proposed by Zhao *et al.*[3] The saturation level of the dislocations δ_{BH} is given by

$$\delta_{\mathrm{BH}} = \frac{N(t)}{N_0} = \frac{1 - \exp\left[3 \cdot (\rho_{f_x} - n_0 a) \cdot \left(\frac{\pi}{2}\right)^{1/3} \left(\frac{ADt}{\mathrm{k}T}\right)^{2/3}\right]}{1 - \frac{N_0}{n_0} \cdot \exp\left[3 \cdot (\rho_{f_x} - n_0 a) \cdot \left(\frac{\pi}{2}\right)^{1/3} \left(\frac{ADt}{\mathrm{k}T}\right)^{2/3}\right]} \qquad [4]$$

where $N(t)$ is the number of solute atoms per unit volume that have reached the dislocation after a time t (N in m^{-3}), N_0 is the number of initial dislocation sites (m^{-3}), A is the interaction energy between the dislocation and the carbon atoms, k is the Boltzmann constant, T is the absolute aging temperature, t is the aging time. The coefficient a represents the dislocation slip distance divided by the number of carbon atoms per atom plane, which is 15 in the model. The term ρ_{f_x} is the dislocation density after x pct prestrain (Eq. [2]), and n_0 is the number of solute atoms in the matrix so that $N_0 = \rho_{f_x}/a$. The diffusion coefficient of carbon in ferrite D ($\mathrm{m}^2 \cdot \mathrm{s}^{-1}$) is given by $D = 2 \cdot 10^{-6} e^{-84{,}018/\mathrm{R}T}$, with R being the gas constant.

It was recently shown by Zhao *et al.*[3] that, for short aging treatments, the ratio $\Delta\sigma/\Delta\sigma_{\max}$, which represents the yield strength increase after aging over the maximum possible strength increase, tends linearly to 1 as the saturation level δ_{BH} approaches unity. This reflects the reality of strain aging kinetics, because the carbon atom that arrives at a dislocation first is more effective in anchoring it than those that arrive later.

For high aging temperatures or long aging times, a second hardening phenomenon actually takes place. This phenomenon is characterized by the increase of both yield strength and yield point elongation. Experiments and literature also show that this second hardening stage tends to increase with solute carbon content and to decrease with prestrain. Its physical mechanism is not well known. This second step may be due to a kind of densification of atmospheres where solute carbon could aggregate into clusters, but these precipitates have not been observed.[14–16] Some other explanations are possible: according to Leslie and Keh,[16] this second step corresponds to the pinning of new dislocation sources in the grain boundaries in the same way as the pinning during the first step by short diffusion of carbon atoms.

This hardening phenomenon has to be taken into account, because the classic paint process, 20 minutes at 170 °C, corresponds to the beginning of this second step. In the present model, it is assumed that the second stage corresponds to a densification of Cottrell atmospheres by precipitation. The growth of precipitates depends on the carbon content segregated at the end of the first step per dislocation unit length. The evolution of the radius of precipitates is given by

$$\frac{dR}{dt} = D \cdot \frac{C_{\mathrm{seg}}^{at} - 0.5 \cdot (R/\Delta)^3}{0.5 \cdot R} \qquad [5]$$

where R is the radius of the precipitates, D is the diffusion coefficient of carbon in ferrite, Δ is the interprecipitate distance, and C_{seg}^{at} is the carbon content segregated at the end of the first step per dislocation unit length:

$$C_{\mathrm{seg}}^{at} = C_0^{at} \cdot \frac{I\Delta}{\rho_{f_x}} \qquad [6]$$

where C_0^{at} is the total carbon content segregated at the end of the first step, I is the nucleation site density, and ρ_{f_x} is the dislocation density after x pct prestrain. The hardening is supposed to be due to the shear of precipitates by dislocations, which is proportional to $(\lambda \cdot R)^{1/2}$, where λ is the precipitate volume fraction (proportional to R^3). By normalizing the radius of precipitates by its maximum value, a saturation level of dislocations by precipitates can be written, in an analogous way to the first aging step:

$$\delta_{\mathrm{prec}} = \frac{R^2}{R_{\max}^2} \qquad [7]$$

so that the second hardening can be written as a linear function of δ_{prec}.

The influence of these two phenomena on the resulting BH has been studied quantitatively.[14,17,18] The result is that BH can be described as a sum of two terms corresponding to the two steps described previously:

$$\mathrm{BH} = \delta_{\mathrm{BH}} \cdot \Delta\sigma_{\max}^{\mathrm{BH}} + \delta_{\mathrm{prec}} \cdot \Delta\sigma_{\max}^{\mathrm{prec}} \quad [8]$$

where $\Delta\sigma_{\max}^{\mathrm{BH}}$ and $\Delta\sigma_{\max}^{\mathrm{prec}}$ are constants to be estimated for each kind of steel.

The predictions of the model are compared with *BH* experimental results. Figure 2 presents the experimental and modeled evolutions of *BH* for the AlK steels with 20 and 60 ppm of solute carbon, aged at 120 °C and 170 °C. Once the parameters $\Delta\sigma_{\max}^{\mathrm{BH}}$ and $\Delta\sigma_{\max}^{\mathrm{prec}}$ of Eq. [8] are identified, the predictions of the model are in good agreement with the experimental data. The two stages of aging are particularly enlightened.

High solute carbon content gives an acceleration of the kinetics, because more carbon is available to pin the dislocations. It also leads to an increase of the second hardening phenomenon, which depends on the carbon segregated at the end of the first step. The effect of the *BH* temperature is also illustrated: high temperatures accelerate the aging kinetics, but do not have any influence on the *BH* saturation level.

The model also takes into account the amount of prestrain. The first aging stage does not present any marked dependency with the prestrain level.[19] The amount of carbon necessary to saturate all the dislocations is, in fact, very small, of the order of a few parts per million. This finding means that, usually, $\rho_{f_x} = n_0 a$ and Zhao kinetics can be substituted by the Harper model (Eq. [4]). Yet, the prestrain level has an influence on the second aging stage.[14,18] As the dislocation density increases, the number of carbon atoms required to saturate the dislocations increases, leaving fewer atoms in solution for the formation of precipitates. This effect is represented in Eq. [6] because the carbon content segregated at the end of the first step by dislocation length unit is considered. The effect of prestrain was confirmed by the measurements of BH after 2 and 5 pct prestrain on ULC steel.

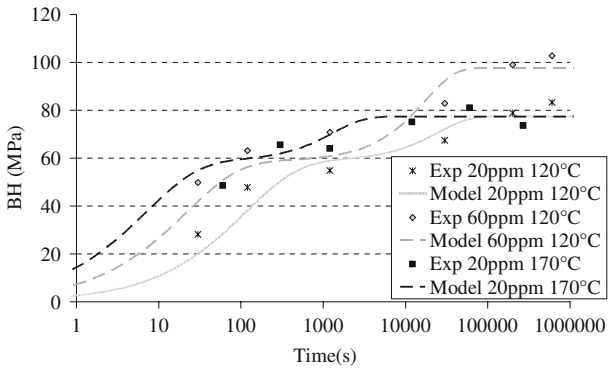

Fig. 2—Experimental evolutions of BH and prediction of the model for AlK steels with 20 and 60 ppm of solute carbon content, aged at 120 °C and 170 °C.

B. *Numerical Approach of the Piobert–Lüders Phenomenon*

The Piobert–Lüders behavior is a propagative plastic instability that occurs particularly during tensile tests in aged steels. It leads to the formation of bands on the sample and gives a plateau on the macroscopic stress-strain curve, characterized by a lower yield stress and a yield point elongation. This particular behavior can be simulated by the FE method.[20,21] Tsukahara and Iung introduced a local behavior with two straight lines, decreasing then increasing, to model the physical basis of the phenomenon. The same idea is used in this work, but an exponential local behavior is introduced here:

$$R = R_0 + Q_1 \cdot \left(1 - e^{-b_1 \cdot \varepsilon_p}\right) + Q_2 \cdot \left(1 - e^{-b_2 \cdot \varepsilon_p}\right) \quad [9]$$

with R_0 being the yield strength; and Q_1, Q_2, b_1, and b_2 being parameters with $Q_1 > 0$ and $Q_2 < 0$. A Voce classic strain hardening behavior[22] is introduced in the first part of the equation. An additional softening term is added with a negative coefficient Q_2 to model static strain aging. The resulting local behavior is shown in Figure 3(b). Its shape allows describing schematically the physics of the Lüders phenomenon. The dislocations are initially locked by solute carbon, and the increase in yield strength represents the stress that has to be overcome to unlock or multiply these dislocations. Once this threshold is overcome, a rapid multiplication of mobile dislocations occurs, which is represented by the decrease of the stress.

Simulations were carried out with two FE codes, Abaqus version 6.34[23] and Z-set,[24] but the choice of FE code does not affect the results. A rectangular mesh of 12.5-mm length and 2.5-mm width under plane stress conditions was considered. A slight defect was introduced in the middle of the left edge in order to initiate the band formation (Lüders bands usually initiate at the shoulders of the testpiece that are stress concentration points). The vertical displacement is fixed to 0 at the bottom. A displacement of 1 mm along the vertical axis is imposed to the head of the specimen.

The result of a uniaxial test performed with 500 reduced quadratic elements is shown in Figure 3(a). It appears that two deformation bands are generated at the defect and propagate along the sample. The angle with the vertical axis is close to 55 deg, which agrees with the theoretical solution under plane stress conditions.[25] The number and the direction of propagation of the bands can vary according to the mesh (random or regular) and to the number of elements, but it does not affect the macroscopic stress-strain response.

Figure 3(b) shows that the propagation of the bands is associated with a plateau on the resulting stress-strain curve, whose length is the Lüders strain ε_L or yield point elongation. It can be noted that the macroscopic response does not follow the local behavior and gives a sharp yield point due to strain localization. Once the bands have propagated along the entire specimen, the deformation becomes homogenous again and the material has a classic uniform work hardening behavior.

It has to be noticed that the level of the macroscopic stress σ_L of the plateau is not equal to $\sigma_{\max}$ nor $\sigma_{\min}$ but

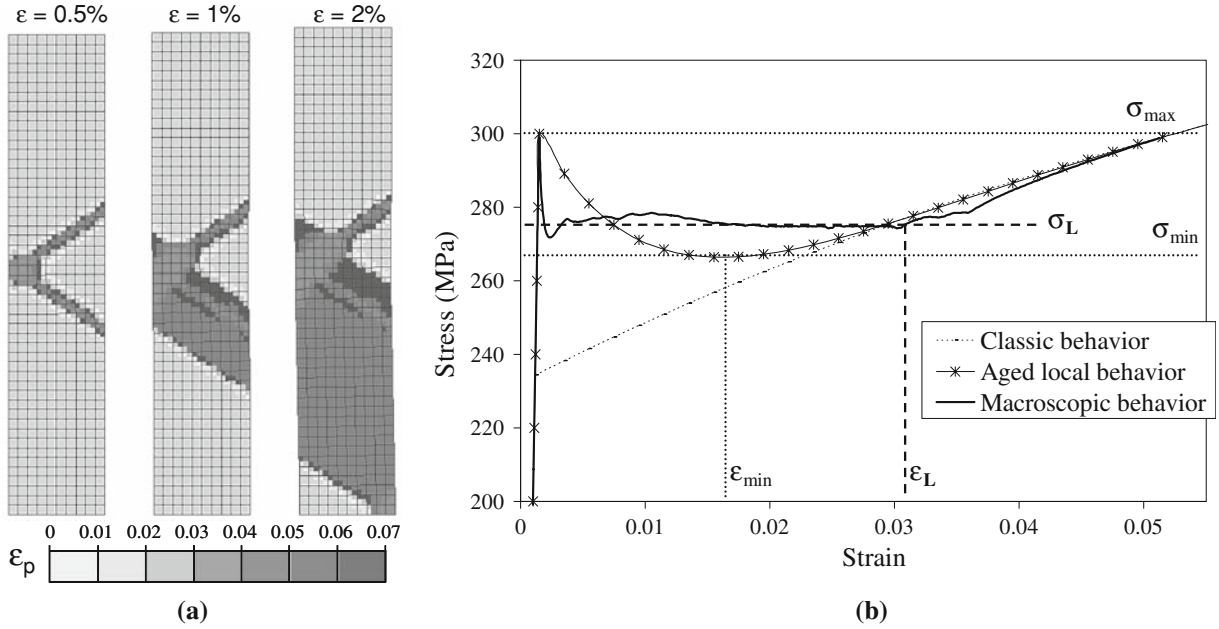

Fig. 3—Simulation of the Lüders behavior. (*a*) Lüders band propagation: three plastic equivalent strain (ε_p) maps for different macroscopic strains: ε = 0.5, 1, and 2 pct. (*b*) Local behavior and resulting stress-strain curve. Simulation for R_0 = 300 MPa, Q_1 = 140 MPa, b_1 = 20, Q_2 = –90 MPa, and b_2 = 100.

lies between these bounds (Figure 3(b) for a definition of these parameters). This level σ_L determines the Lüders strain ε_L, given by the constitutive law. The study of a band showed that the strain profile in the band is constant and equal to ε_L and the stress is close to the macroscopic Lüders stress σ_L, which agrees with the literature.[20]

The influence of σ_{max}, σ_{min}, and ε_{min} on the Lüders variables σ_L and ε_L has been investigated. Simulations were conducted using the same type of local behavior with an exponential shape. The results show that the Lüders stress is related to the difference between the maximum and the minimum of the local behavior:

$$\sigma_L - \sigma_{min} = \frac{1}{4}(\sigma_{max} - \sigma_{min}) \qquad [10]$$

Once the Lüders stress is determined, the Lüders strain is given by the constitutive law. However, other simulations carried out with a bilinear local behavior instead of a double exponential one lead to a different relation:

$$\sigma_L - \sigma_{min} = 0.4 \cdot (\sigma_{max} - \sigma_{min}) \qquad [11]$$

which is close to the value found by Tsukahara *et al.*[20]

A particular simulation was conducted with triangular linear elements oriented in the same direction as the band (*i.e.*, with an angle of 55 deg with the vertical axis), as shown in Figure 4(a). In that case, the band front is well delimited by the element edges and corresponds to a line of elements. Such a simulation does not give a plateau but oscillations in the macroscopic response (Figure 4(b)). Each oscillation, which varies between σ_{max} and σ_{min}, occurs at each time when the band propagates from a line of elements to another. This particular behavior is due to the possibility for the FE code to accommodate the strain discontinuity thanks to these oriented elements. When using classic elements, the band front is not clearly defined and the FE code accommodates the strain discontinuity by creating shear stresses. As a consequence, the plateau stress only represents the result of a numerical artifact necessary for the computation of strain discontinuity.

Thus, the macroscopic responses of simulations are dependent of both the shape of the local behavior and the FE type, particularly for oriented triangular elements. In order to eliminate these numerical dependences, it was decided to always use the same shape of local behavior and the same kind of elements. An exponential local behavior was considered in order to determine the value of the simulated plateau stress as a function of the parameters of Eq. [10]. Standard square or triangular elements (but not oriented) were used, because they do not have any influence on the results. Simulations do not mark any dependency with the size of elements either, allowing reproduction of the Lüders plateau, which is observed experimentally, and simulation of this phenomenon in a predictive way (Eq. [10]).

C. *Coupling with the Strain Aging Model*

The previous simulations of the Lüders phenomenon are now coupled with the model of the strain aging kinetics in order to predict and simulate BH tensile tests. Standard BH tests correspond to a load to 2 pct strain in uniaxial tension, aging treatment, and then loading in the same direction as prestrain. To simulate such a test, an extra hardening term analogous to the one described previously is introduced and illustrated in Figure 5.

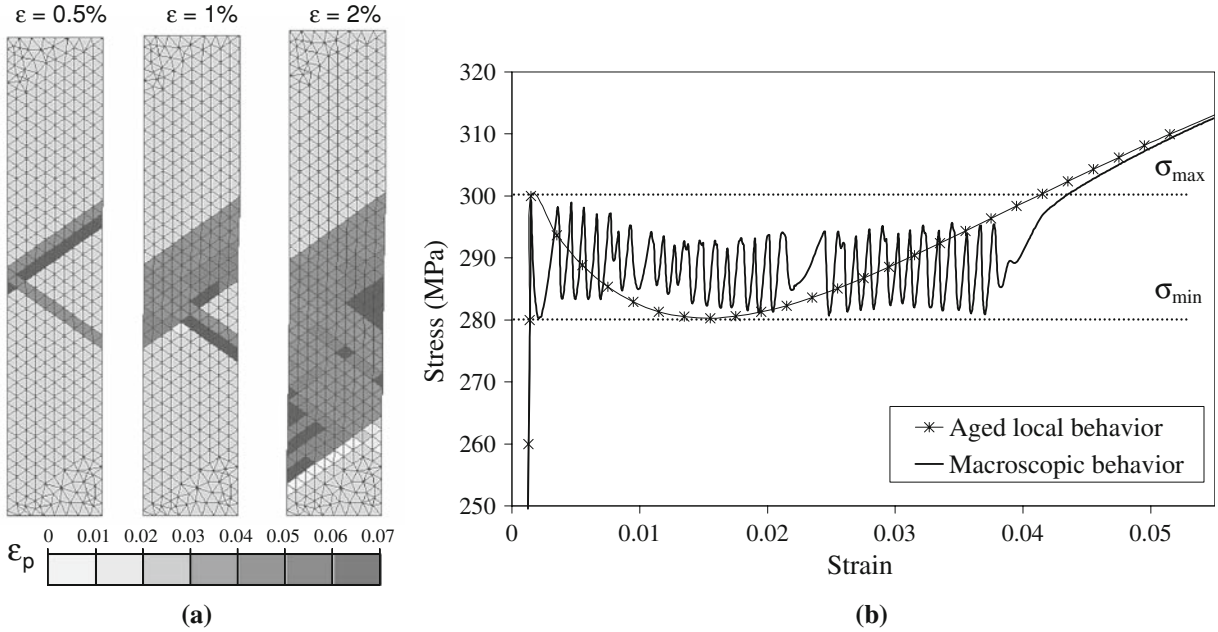

Fig. 4—Simulation of the Lüders behavior. (*a*) Lüders band propagation: three plastic equivalent strain (ε_p) maps for different macroscopic strains: ε = 0.5, 1, and 2 pct. (*b*) Local behavior and resulting stress-strain curve. Simulation for R_0 = 300 MPa, Q_1 = 140 MPa, b_1 = 20, Q_2 = –80 MPa, and b_2 = 80.

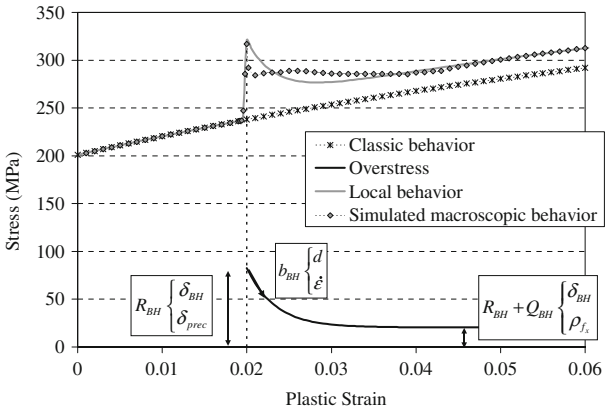

Fig. 5—Example of simulations of classic and aged behaviors. Shape and parameters of the overstress are specified. The local behavior introduced in the simulation is the sum of the classic behavior and the overstress.

The equation of the overstress is given by

$$\sigma_{\mathrm{BH}} = R_{\mathrm{BH}} + Q_{\mathrm{BH}} \cdot \left(1 - e^{-b_{\mathrm{BH}} \cdot \left(\varepsilon^p - \varepsilon^p_{\mathrm{prestrain}}\right)}\right) \qquad [12]$$

The first parameter R_{BH} determines the value of the sharp yield point. It is assumed that the dislocation saturation level will affect the coefficient R_{BH}, because the longer the aging treatment, the higher the BH level, as shown by Eq. [10]. The term R_{BH} is then considered as a linear function of BH determined by Eq. [8], that is to say proportional to δ_{BH} and δ_{prec}. The value of this coefficient is fixed to

$$R_{\mathrm{BH}} = 1.6 \cdot \mathrm{BH} = 1.6 \cdot \left(\delta_{\mathrm{BH}} \cdot \Delta\sigma^{\mathrm{BH}}_{\max} + \delta_{\mathrm{prec}} \cdot \Delta\sigma^{\mathrm{prec}}_{\max}\right) \qquad [13]$$

Experiments and literature show that the existence and the value of the sharp yield point depends strongly on the testing procedure, so that the value of the proportionality coefficient here fixed to 1.6 remains imprecisely known. However, this is not limitative.

The value of the asymptote is not zero and depends on the aging treatment. This modification of the classic hardening behavior after the Lüders phenomenon has been particularly investigated by Soler.[14] He showed that the gap between the aged and the classic behaviors increases with time and temperature of the aging treatment until a saturation. The evolution of this phenomenon can actually be correlated with the first step of the BH mechanisms described previously. The gap increases linearly with δ_{BH} and remains constant once the first stage of aging saturates, that is to say when δ_{BH} = 1. The second hardening phenomenon due to densification of Cottrell atmospheres has no influence on the material behavior after the Lüders plateau. Soler also showed that the difference between aged and classic behaviors depends on prestrain; an increase of prestrain leads to an increase of the gap. It is then assumed that

$$\Delta\sigma_{\varepsilon_p = \varepsilon_L} = \sigma_{\mathrm{BH}}\left(\varepsilon_p = \varepsilon_L\right) = R_{\mathrm{BH}} + Q_{\mathrm{BH}} = K \cdot \rho_{f_x} \cdot \delta_{\mathrm{BH}} \qquad [14]$$

where K is a constant. The parameter Q_{BH} is then deduced from the two previous Eqs. [13] and [14].

The effects of grain size and strain rate on BH and yield point elongation have widely been investigated in the literature.[8,26,27] It has been shown that small grain sizes or high strain rates lead to an increase of both lower yield stress and yield point elongation. Grain size

actually has an influence on the velocity of the Lüders band front. Grain boundaries act as obstacles to the front propagation, so that they control the Lüders band velocity. Thus, a small grain size will make the band propagation more difficult and lead to a higher value of lower yield stress and yield point elongation. Quantitative analyses in the literature[8] showed that the effect of grain size on the lower yield stress can be described by a Hall–Petch type relation. The explanation of the effect of strain rate is analogous to the previous one, but no relation between strain rate and the lower yield stress has been generally admitted.

To take these effects into account in the model, grain size and strain rate are introduced in the definition of coefficient b_{BH}. This coefficient is responsible for the initial slope of the softening branch of the material behavior law and allows indirect representation of the grain size and strain rate effects on band propagation. The following equation is introduced to determine b_{BH}:

$$b_{BH} = K_d \cdot d^{0.8} - S \cdot \ln\left(\frac{\dot{\varepsilon}}{\dot{\varepsilon}_0}\right) \qquad [15]$$

where d is the grain size; $\dot{\varepsilon}$ is the strain rate; and K_d, S, and $\dot{\varepsilon}_0$ are constants. The effect of grain size appears with $d^{0.8}$ in order to give a linear relation between the lower yield stress and $d^{-1/2}$ when considering BH steel standard behaviors. The terms K_d and S are fitted to give, in relation with Eqs. [10] and [13], a good prediction of the BH level for a standard test. The strain rate is directly introduced *via* a logarithmic relation.

IV. RESULTS AND DISCUSSION

Finite element simulations were performed and compared with experimental macroscopic curves obtained for AlK and ULC steels. The FE codes and elements were the same as for the simulation presented in Figure 3. The "as-received" behavior was fitted with a Voce type hardening behavior.[22] The influence of the aging treatment was then modeled with an extra hardening term, as described previously.

The experimental and simulated behaviors of an AlK steel aged at 120 °C for different aging times are presented in Figure 6. Experiments show the increase in Lüders stress and Lüders strain for an increasing aging time. It can be noted that the macroscopic behavior of an aged steel is well reproduced by the model. The lower yield stress, the yield point elongation, and their dependence with aging time are particularly well predicted.

A validation of the implementation of the grain size effect is also proposed. Tensile tests are performed of the three AlK steels with different grain sizes (d = 8, 13, and 30 μm) but with the same solute carbon content (20 ppm). Thus, the carbon available to pin the dislocations is the same for the three modalities. Figure 7 shows the experimental and simulated macroscopic responses of these materials after 2 pct prestrain and a classic aging treatment (170 °C, 20 minutes). The experimental macroscopic behavior is not the same during prestrain due to the difference of grain size. However, it can be noted that a small grain size leads to a higher value of BH and Lüders strain. The effect of grain size in the simulations was introduced in the initial slope of the local behavior, as described previously (b_{BH} coefficient

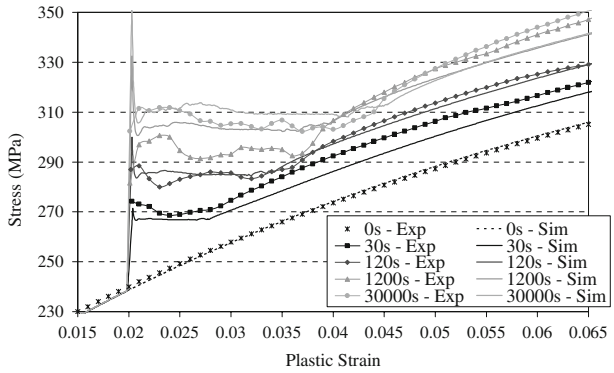

Fig. 6—Experimental and simulated stress-strain curves of an AlK steel aged at 120 °C for 0 (as received), 30, 120, 1200, and 30,000 s.

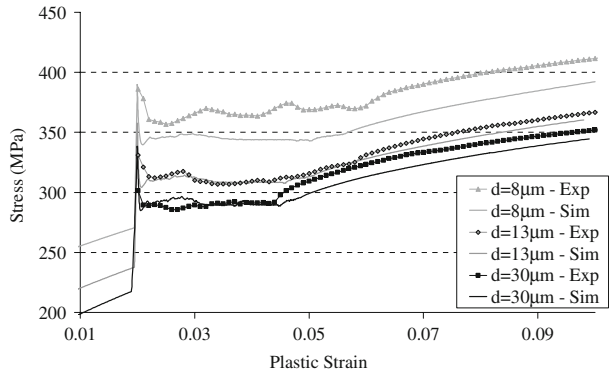

Fig. 7—Experimental and simulated stress-strain curves of three AlK steels with d = 8, 13, and 30 μm, aged at 170 °C for 1200 s.

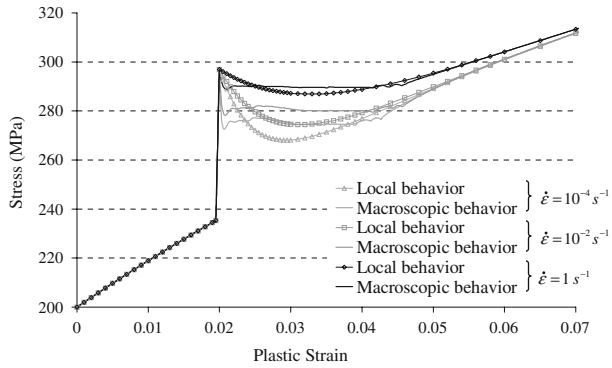

Fig. 8—Local behaviors and simulated macroscopic behaviors for three different strain rates: $\dot{\varepsilon} = 10^{-4}, 10^{-2}$ and 1 s^{-1}. The as-received behavior does not have a viscous behavior in the simulations; strain rate effect is introduced only for aged behaviors.

in Eq. [15]). This effect on yield point elongation is well reproduced by the model.

The strain rate effect is illustrated in Figure 8, which shows the local constitutive laws introduced in the FE code and the simulated macroscopic responses obtained for three different strain rates. For a given initial behavior, an increase in strain rate leads to higher yield strengths and yield point elongations. This effect was not validated with experimental data, but it agrees qualitatively well with the literature.[7,27]

V. CONCLUSIONS

A modeling of the behavior of BH steels has been developed. This model was based on experiments carried out on two BH steels. The effects of solute carbon content, grain size, prestrain, and aging treatment have been particularly studied. A detailed description of the kinetics of aging has been developed, composed of the formation of Cottrell atmospheres and precipitation of carbides. This description was then coupled with a numerical approach of the Piobert–Lüders phenomenon. Finite element simulations of tensile tests were performed and compared with experiments, which led to the following results.

1. The strain aging model has been validated for two steels. Both stages of the kinetics are well predicted and the effect of prestrain on the precipitation of carbides is taken into account.
2. Simulations predict particularly well the BH, the yield point elongation, and their dependence with the aging treatment. The propagation of Piobert–Lüders bands and the apparition of a sharp yield point and a plateau on the macroscopic response are reproduced.
3. The effects of grain size and strain rate are particularly enlightened. The model allows taking into account the influence of these parameters on band propagation and reproduction of their effects on the macroscopic response.

ACKNOWLEDGMENT

The authors are grateful to J.L. Uriarte and O. Bouaziz for helpful discussions.

REFERENCES

1. A.H. Cottrell and B.A. Bilby: *Proc. Phys. Soc.*, 1949, vol. 62, pp. 49–62.
2. A.K. De: Ph.D. Thesis, Ghent University, Ghent, Belgium, 2000.
3. J.Z. Zhao, A.K. De, and B.C. De Cooman: *Metall. Mater. Trans. A*, 2001, vol. 32A, pp. 417–23.
4. G.T. Hahn: *Acta Metall.*, 1962, vol. 10, pp. 727–38.
5. F. Garofalo: *Metall. Trans.*, 1973, vol. 4, pp. 1557–61.
6. P. Hähner: *Appl. Phys.*, 1994, vol. A58, pp. 41–48.
7. F. Yoshida: *Int. J. Plast.*, 2000, vol. 16, pp. 359–80.
8. J.F. Butler: *J. Mech. Phys. Solids*, 1962, vol. 10, pp. 313–34.
9. V. Ballarin, A. Perlade, S. Forest, and X. Lemoine: *Metall. Mater. Trans. A*, 2006, vol. 37A, DOI 10.1007/s11661-009-9812-6.
10. S. Harper: *Phys. Rev.*, 1951, vol. 83, pp. 709–12.
11. D. Mac Lean: *Grain Boundaries in Metals*, Oxford University Press, Oxford, United Kingdom, 1957.
12. Y. Bergström: *Mater. Sci. Eng.*, 1969, vol. 5, pp. 193–200.
13. U.F. Kocks: *J. Eng. Mater. Technol.*, 1976, vol. 98, pp. 76–85.
14. M. Soler: Ph.D. Thesis, Institut National des Sciences Appliquées de Lyon, Lyon, France, 1998 (in French).
15. J.M. Rubianes and P. Zimmer: *Rev. Metall. Cah. Inf. Technol.*, 1996, pp. 99–109.
16. W.C. Leslie and A.S. Keh: *J. Iron Steel Inst.*, 1962, vol. 200, pp. 722–28.
17. P. Elsen and H.P. Hougardy: *Steel Res.*, 1993, vol. 64, pp. 431–36.
18. L.J. Baker, J.D. Parker, and S.R. Daniel: *Mater. Sci. Technol.*, 2002, vol. 18, pp. 541–47.
19. A.K. De, K. De Blauwe, S. Vandeputte, and B.C. De Cooman: *J. Alloys Compd.*, 2000, vol. 310, pp. 405–10.
20. H. Tsukahara and T. Iung: *Mater. Sci. Eng. A*, 1998, vol. 248, pp. 304–08.
21. S. Graff, S. Forest, J.-L. Strudel, C. Prioul, P. Pilvin, and J.-L. Béchade: *Mater. Sci. Eng. A*, 2004, vols. 387–389, pp. 181–85.
22. E. Voce: *J. Inst. Met.*, 1948, vol. 74, pp. 537–62.
23. *Abaqus*, 2004, www.abaqus.com.
24. *Z-set*, 2001, www.nwnumerics.com, www.mat.ensmp.fr.
25. J. Besson, G. Cailletaud, J.-L. Chaboche, and S. Forest: *Mécanique Non Linéaire des Matériaux*, Hermès, Paris, 2001, pp. 385–420 (in French).
26. D.V. Wilson: *Acta Metall.*, 1968, vol. 16, pp. 743–53.
27. H. Fujita and S. Miyazaki: *Acta Metall.*, 1978, vol. 26, pp. 1273–81.